Nonlinear Dyn (2014) 77:655–666
DOI 10.1007/s11071-014-1328-y

ORIGINAL PAPER

Partially saturated nonlinear control for gantry cranes with hardware experiments

Ning Sun · Yongchun Fang

Received: 26 February 2013 / Accepted: 21 February 2014 / Published online: 12 March 2014

Abstract Gantry cranes are typically underactuated nonlinear dynamic systems with highly coupled system states. We propose in this paper a partially saturated nonlinear controller for gantry crane systems by converting the crane model into an objective (i.e., desired closed-loop) system. The presented scheme guarantees "soft" cart start by introducing a smooth saturated function into the controller. In particular, we first establish an objective system with desired signal convergence and stability performance. Then, on the basis of the objective dynamics' structure, we derive a partially saturated control law straightforwardly by solving one partial differential equation, without necessity of performing partial feedback linearization operations to the original crane model. The convergence and stability performance of the objective system is assured with Lyapunov-based methods. In order to verify the practical control performance of the proposed method, we implement both numerical simulation and hardware experiments to illustrate that the new method achieves increased performance with respect to existing methods, with lessened control efforts.

Keywords Nonlinear control · Gantry cranes · Objective system · Partially saturated

N. Sun · Y. Fang (✉)
Institute of Robotics and Automatic Information System, Nankai University, Tianjin, China
e-mail: yfang@robot.nankai.edu.cn

N. Sun
e-mail: sunn@robot.nankai.edu.cn

1 Introduction

Nonlinear underactuated mechatronic systems, including cranes, nonholonomic mobile robots, underactuated helicopters and vessels, etc., are playing an increasingly important role in real-world applications. For these systems, high nonlinearity and strong states coupling are usually present. Moreover, the basic property of such systems that more degrees-of-freedom (DOFs) need to be dominated by less control inputs brings further challenge for their controller development. It is hence a hot research topic attracting much attention [1–11]. Gantry cranes, as powerful industrial tools, belong to the classification of underactuated systems with complicated nonlinear dynamics. The control problem for controlling cranes is important yet challenging, for which a considerable amount of studies have been done to improve the control system performance. Linear control methods, such as optimal control [12,13], trajectory planning [14,15], input shaping [16,17], delayed feedback control [18], fuzzy PID control [19], etc., have been developed to achieve satisfactory performance. However, if the underactuated load exhibits large-amplitude swinging motion, the performance of these linearization-based methods may possibly degrade. Hence, nonlinear crane control techniques are employed, which can be mainly classified as energy-based methods [20,21], nonlinear motion planning [22,23], saturation control [24,25], sliding mode approaches [26–30], partial feedback linearization-based method [31], and so on. In addi-

tion to the control methods mentioned previously, many researchers also apply the intelligent strategies including genetic algorithms (GA) [32], neural networks (NN) [33], and fuzzy logic control [34], to optimize and improve the performance of the crane control systems.

For existing (crane) regulation/stabilization methods, the regulation/stabilization errors are usually defined as the differences between the current state variables (cart displacement) and their desired values (desired cart location) [8–11,20,21,26,35,36]. Thus, one potential issue is that the initial computed control force relies greatly on the transportation distance (i.e., the initial positioning error). For a set of control gains properly tuned for a specific transferring distance, when the desired location gets farther in a different transportation process, the control force (especially the initial force) will become much larger and may cause damages to the actuating motors. Moreover, the corresponding large cart acceleration will excite large-amplitude load swing angle, which is unexpected in practice. One possible way to address this problem is to retune the control gains when the desired location changes, but it is cumbersome since tuning such nonlinear control systems as cranes are usually complicated and there are currently no general guidelines available.

This paper proposes a partially saturated nonlinear control scheme for underactuated gantry cranes, which achieves superior control performance and guarantees "soft" cart start, and a set of properly chosen control gains works well for different transportation processes of different distances, with less consumed control efforts. It is known that the derivations for most crane control methods, such as those in [20,21,24–30,35], are established by fabricating a Lyapunov function and then taking its time derivative (to design the control law). Different from these methods, by borrowing ideas from the innovative and constructive energy-shaping technique [37], we alternatively construct a desired objective (i.e., closed-loop) system with some specific structure and then obtain a control law capable of converting the original crane dynamics to the objective system. We have also introduced a smooth saturated function into the control law to successfully reduce the control efforts, especially the initial control forces. The stability and signal convergence performance are rigorously supported by Lyapunov-based techniques. The proposed method is implemented both numerically in the environment of MATLAB/SIMULINK and experimentally on a hardware gantry crane testbed, which confirms that the proposed scheme can achieve superior performance over existing schemes, in terms of better swing suppression, reduced control efforts, and increased robustness. In addition, the verification results also illustrate that, for the proposed method, one does not need to retune the control gains when the transportation distance changes (becomes longer)—which brings much convenience for practical implementation.

The contents of the paper are organized as follows. The problem formulation is introduced in details in Sect. 2. In Sect. 3, we construct an objective crane system and then derive the control law. We prove the asymptotic stability for the equilibria of the closed-loop (objective) system in Sect. 4. Section 5 exhibits both numerical simulation and hardware experimental results. Finally in Sect. 6, some conclusions and discussions are provided.

2 Problem formulation

Let us consider an underactuated gantry crane system with the following dynamics [14,22]:

$$\boldsymbol{M}(\boldsymbol{q})\ddot{\boldsymbol{q}} + \boldsymbol{V}_m(\boldsymbol{q},\dot{\boldsymbol{q}})\dot{\boldsymbol{q}} + \boldsymbol{G}(\boldsymbol{q}) = \boldsymbol{u}, \tag{1}$$

where $\boldsymbol{q}(t) = [x(t)\theta(t)]^{\mathrm{T}} \in \mathbb{R}^2$ denotes the system state vector with $x(t)$ and $\theta(t)$ being the cart displacement and the load swing angle, respectively; and $\boldsymbol{M}(\boldsymbol{q})$, $\boldsymbol{V}_m(\boldsymbol{q},\dot{\boldsymbol{q}}) \in \mathbb{R}^{2\times 2}$, $\boldsymbol{G}(\boldsymbol{q})$, and $\boldsymbol{u} \in \mathbb{R}^2$ represent the inertia matrix, the centripetal-Coriolis matrix, the gravity vector, and the control input vector, respectively; they are explicitly defined as

$$\boldsymbol{M} = \begin{bmatrix} M+m & ml\cos\theta \\ ml\cos\theta & ml^2 \end{bmatrix}, \quad \boldsymbol{V}_m = \begin{bmatrix} 0 & -ml\sin\theta\dot{\theta} \\ 0 & 0 \end{bmatrix}, \tag{2}$$

$$\boldsymbol{G} = [0\ mgl\sin\theta\,]^{\mathrm{T}}, \quad \boldsymbol{u} = [\,F\ 0\,]^{\mathrm{T}} \triangleq \boldsymbol{\varphi}F, \tag{3}$$

where M represents the cart mass, m represents the load mass, l is the cable length, $\boldsymbol{\varphi}$ is denoted by

$$\boldsymbol{\varphi} = [\,1\ 0\,]^{\mathrm{T}},$$

and $F(t)$ represents the resultant force imposed on the cart consisting of the following two parts:

$$F = F_{\mathrm{a}} - F_{\mathrm{r}},$$

wherein $F_a(t)$ denotes the actuating force and $F_r(t)$ is the bridge friction force. In this paper, the following friction force model, which is similar to the one proposed in [38], is used to describe the bridge friction force [22]:

$$F_r(\dot{x}) = F_{r0}\tanh(\dot{x}/\varepsilon) - k_r|\dot{x}|\dot{x}, \tag{4}$$

with $F_{r0}, k_r, \varepsilon \in \mathbb{R}$ denoting friction-related parameters.[1] Using (2) and (3), the crane dynamics (1) can be written in the following manner:

$$(M+m)\ddot{x} + ml\ddot{\theta}\cos\theta - ml\dot{\theta}^2\sin\theta = F_a - F_r, \tag{5}$$

$$l\ddot{\theta} + \cos\theta\ddot{x} + g\sin\theta = 0. \tag{6}$$

The control objective is to develop a control law capable of regulating all the system state variables to the equilibria; that is, the cart is driven to arrive at the desired location while the unexpected load swing is effectively suppressed and eliminated simultaneously in the sense that

$$\boldsymbol{e}(t) = [x - x_d \;\; \theta]^{\mathrm{T}} \triangleq [e_x \;\; \theta]^{\mathrm{T}} \to [0 \;\; 0]^{\mathrm{T}}, \tag{7}$$

where $x_d \in \mathbb{R}$ denotes the desired cart position, $\boldsymbol{e}(t) \in \mathbb{R}^2$ denotes regulation error vector, and $e_x(t) \in \mathbb{R}$ is the cart positioning error signal. Then, it is easily deduced from (7) that

$$\dot{\boldsymbol{e}}(t) = \dot{\boldsymbol{q}}(t) = [\dot{x} \;\; \dot{\theta}]^{\mathrm{T}}, \;\; \ddot{\boldsymbol{e}}(t) = \ddot{\boldsymbol{q}}(t) = [\ddot{x} \;\; \ddot{\theta}]^{\mathrm{T}} \tag{8}$$

which, together with (1) and (3), indicates that

$$\boldsymbol{M}(\boldsymbol{q})\ddot{\boldsymbol{e}} = -\boldsymbol{V}_m(\boldsymbol{q}, \dot{\boldsymbol{e}})\dot{\boldsymbol{e}} - \boldsymbol{G}(\boldsymbol{q}) + \boldsymbol{\varphi}F. \tag{9}$$

In the next section, we will exploit a suitable control law that achieves the control objective of (7).

3 Controller development

We will establish an objective crane system with desired (stability) performance in this section. After that, an appropriate control law will be developed to convert the crane dynamics into the desired objective system.

[1] We focus our controller development on the resultant force $F(t)$ since, in this work, the model (4) will be utilized for feedforward friction force compensation, as will be shown in the experiments in Sect. 5.

3.1 Objective system construction

In order to achieve the control objective of (7), we are motivated to seek for a proper control signal $\boldsymbol{u}(t)$, so that the system's open-loop dynamics can be converted into a closed-loop form with an unique asymptotically stable equilibrium point at the desired state. Toward this end, we want to construct an objective system by respecting the following two basic principles: (1) the equilibrium point of the objective system should be asymptotically stable and (2) the structure of the designed objective system ought to be similar to that of the original crane dynamics so that the system matching operations are easy to carry out. According to the foregoing two points, based on the Euler–Lagrange structure of (9), we construct the following desired objective system:

$$\boldsymbol{M}_d\ddot{\boldsymbol{e}} + \boldsymbol{\Lambda}_d\dot{\boldsymbol{e}} + \frac{\partial P_d(\boldsymbol{e})}{\partial \boldsymbol{e}} = 0, \tag{10}$$

where $\boldsymbol{M}_d \in \mathbb{R}^{2\times 2}$ is a positive definite constant matrix denoting the desired inertia matrix, $\boldsymbol{\Lambda}_d \in \mathbb{R}^{2\times 2}$ is a *positive semi-definite* matrix that denotes the damping matrix, and $P_d(\boldsymbol{e}) \in \mathbb{R}^+$ represents the desired objective potential energy. In addition, the following conditions are satisfied: $(1/2)\dot{\boldsymbol{e}}^{\mathrm{T}}\boldsymbol{M}_d\dot{\boldsymbol{e}} + P_d(\boldsymbol{e})$ is positive definite with respect to $\boldsymbol{e}(t)$, $\dot{\boldsymbol{e}}(t)$ and has a minimum at the equilibrium point. Then, the following proposition can be obtained correspondingly.

Proposition 1 *The objective system (10) is Lyapunov stable at the equilibrium point.*

Proof Consider the following positive definite scalar function:

$$V(t) = \frac{1}{2}\dot{\boldsymbol{e}}^{\mathrm{T}}\boldsymbol{M}_d\dot{\boldsymbol{e}} + P_d(\boldsymbol{e}). \tag{11}$$

Taking its time derivative along the trajectories of (10) produces the following result:

$$\dot{V}(t) = \dot{\boldsymbol{e}}^{\mathrm{T}}\left(\boldsymbol{M}_d\ddot{\boldsymbol{e}} + \frac{\partial P_d(\boldsymbol{e})}{\partial \boldsymbol{e}}\right) = -\dot{\boldsymbol{e}}^{\mathrm{T}}\boldsymbol{\Lambda}_d\dot{\boldsymbol{e}} \le 0. \tag{12}$$

Hence, the equilibrium point is stable in the sense of Lyapunov. □

In view of Proposition 1, if the damping matrix $\boldsymbol{\Lambda}_d$ is chosen appropriately, we can make the equilibrium point asymptotically stable. Motivated by this

fact, we will carefully select proper values for $\boldsymbol{M}_d$, $\boldsymbol{\Lambda}_d$, and $P_d(\boldsymbol{e})$ in the next subsection.

3.2 Objective system matching

By multiplying both sides of (10) with $\boldsymbol{M}_d^{-1}$ and making some mathematical arrangements, we derive that

$$\ddot{\boldsymbol{e}} = -\boldsymbol{M}_d^{-1}\boldsymbol{\Lambda}_d\dot{\boldsymbol{e}} - \boldsymbol{M}_d^{-1}\frac{\partial P_d}{\partial \boldsymbol{e}},$$

which further implies that

$$\boldsymbol{M}(\boldsymbol{q})\ddot{\boldsymbol{e}} = -\boldsymbol{M}(\boldsymbol{q})\boldsymbol{M}_d^{-1}\boldsymbol{\Lambda}_d\dot{\boldsymbol{e}} - \boldsymbol{M}(\boldsymbol{q})\boldsymbol{M}_d^{-1}\frac{\partial P_d}{\partial \boldsymbol{e}}. \quad (13)$$

Substituting (9) into (13) produces the following result:

$$\boldsymbol{V}_m\dot{\boldsymbol{e}} + \boldsymbol{G}(\boldsymbol{q}) - \boldsymbol{\varphi}F = \boldsymbol{M}(\boldsymbol{q})\boldsymbol{M}_d^{-1}\boldsymbol{\Lambda}_d\dot{\boldsymbol{e}} + \boldsymbol{M}(\boldsymbol{q})\boldsymbol{M}_d^{-1}\frac{\partial P_d}{\partial \boldsymbol{e}}, \quad (14)$$

which can be rearranged into the following manner:

$$\boldsymbol{\varphi}F = \boldsymbol{V}_m\dot{\boldsymbol{e}} + \boldsymbol{G}(\boldsymbol{q}) - \boldsymbol{M}(\boldsymbol{q})\boldsymbol{M}_d^{-1}\boldsymbol{\Lambda}_d\dot{\boldsymbol{e}} - \boldsymbol{M}(\boldsymbol{q})\boldsymbol{M}_d^{-1}\frac{\partial P_d}{\partial \boldsymbol{e}}. \quad (15)$$

Since $\boldsymbol{\varphi} = [1 \;\; 0]^{\mathrm{T}}$ is an invertible column vector, the control input $F(t)$ can merely affect the system dynamics within $\boldsymbol{\varphi}$'s range space, namely the actuated part. In other words, for a convertible objective system, the following constraint should be satisfied:

$$\boldsymbol{\varphi}^{\perp}\boldsymbol{\varphi}F = \boldsymbol{\varphi}^{\perp}\left[\boldsymbol{V}_m\dot{\boldsymbol{e}} + \boldsymbol{G}(\boldsymbol{q}) - \boldsymbol{M}(\boldsymbol{q})\boldsymbol{M}_d^{-1}\boldsymbol{\Lambda}_d\dot{\boldsymbol{e}} - \boldsymbol{M}(\boldsymbol{q})\boldsymbol{M}_d^{-1}\frac{\partial P_d}{\partial \boldsymbol{e}}\right] = 0, \quad (16)$$

where $\boldsymbol{\varphi}^{\perp} = [0 \;\; 1]$ represents a left annihilator of $\boldsymbol{\varphi}$. Then, the control force $F(t)$ can be calculated from (15) as

$$F(t) = \boldsymbol{\varphi}^{+}\left[\boldsymbol{V}_m\dot{\boldsymbol{e}} + \boldsymbol{G}(\boldsymbol{q}) - \boldsymbol{M}(\boldsymbol{q})\boldsymbol{M}_d^{-1}\boldsymbol{\Lambda}_d\dot{\boldsymbol{e}} - \boldsymbol{M}(\boldsymbol{q})\boldsymbol{M}_d^{-1}\frac{\partial P_d}{\partial \boldsymbol{e}}\right], \quad (17)$$

where

$$\boldsymbol{\varphi}^{+} \triangleq \left(\boldsymbol{\varphi}^{T}\boldsymbol{\varphi}\right)^{-1}\boldsymbol{\varphi}^{\mathrm{T}} = \boldsymbol{\varphi}^{\mathrm{T}} = \begin{bmatrix} 1 & 0 \end{bmatrix} \quad (18)$$

denotes the left Moore–Penrose pseudo inverse of $\boldsymbol{\varphi}$. Therefore, if $\boldsymbol{M}_d$, $\boldsymbol{\Lambda}_d$, and $P_d(\boldsymbol{e})$ in the objective system (10) are calculated, one can directly obtain the control force $F(t)$ from (17).

Remark 1 It is clear that (17) can be naturally derived from (15). In fact, with $\boldsymbol{M}_d$, $\boldsymbol{\Lambda}_d$, and $P_d(\boldsymbol{e})$ being determined by (16), $F(t)$ satisfying (17) can uniquely imply that (15) holds. To illustrate this point,we will implement some mathematical analyses. For brevity, we denote

$$\boldsymbol{A} = \boldsymbol{V}_m\dot{\boldsymbol{e}} + \boldsymbol{G}(\boldsymbol{q}) - \boldsymbol{M}(\boldsymbol{q})\boldsymbol{M}_d^{-1}\boldsymbol{\Lambda}_d\dot{\boldsymbol{e}} - \boldsymbol{M}(\boldsymbol{q})\boldsymbol{M}_d^{-1}\frac{\partial P_d}{\partial \boldsymbol{e}} \triangleq [a_1 \;\; a_2]^{\mathrm{T}} \in \mathbb{R}^2.$$

Note that by determining $\boldsymbol{M}_d$, $\boldsymbol{\Lambda}_d$, $P_d(\boldsymbol{e})$ from (16), we guarantee that (16) holds. Hence, according to (16) and the fact of $\boldsymbol{\varphi}^{\perp} = [0 \;\; 1]$, we have

$$\boldsymbol{\varphi}^{\perp}\boldsymbol{A} = [0 \;\; 1][a_1 \;\; a_2]^{\mathrm{T}} = a_2 = 0 \Rightarrow \boldsymbol{A} = [a_1 \;\; 0]^{\mathrm{T}}.$$

Substituting $F(t)$ of (17) into the left side of (15) yields

$$\boldsymbol{\varphi}\boldsymbol{\varphi}^{+}\boldsymbol{A} = \begin{bmatrix} 1 & 0 \\ 0 & 0 \end{bmatrix}[a_1 \;\; 0]^{\mathrm{T}} = [a_1 \;\; 0]^{\mathrm{T}} = \boldsymbol{A},$$

which is exactly the equation shown in (15) and hence reveals that, subject to (16), we have (15) $\Longrightarrow$ (17) and (17) $\Longrightarrow$ (15) uniquely.

In order to derive the control force $F(t)$, we need to determine $\boldsymbol{M}_d$, $\boldsymbol{\Lambda}_d$, and $P_d(\boldsymbol{e})$ from (16). However, both ordinary and partial differential equations are involved in (16); hence, to make the problem more convenient to solve, we alternatively decompose it into the following two equations:

$$\boldsymbol{\varphi}^{\perp}\left[\boldsymbol{V}_m\dot{\boldsymbol{e}} - \boldsymbol{M}(\boldsymbol{q})\boldsymbol{M}_d^{-1}\boldsymbol{\Lambda}_d\dot{\boldsymbol{e}}\right] = 0, \quad (19)$$

$$\boldsymbol{\varphi}^{\perp}\left[\boldsymbol{G}(\boldsymbol{q}) - \boldsymbol{M}(\boldsymbol{q})\boldsymbol{M}_d^{-1}\frac{\partial P_d}{\partial \boldsymbol{e}}\right] = 0. \quad (20)$$

To make the equations solvable, we need first to fix one of these three terms. Here, for convenience, we fix the

desired objective inertia matrix $\boldsymbol{M}_d$ of the following expression:

$$\boldsymbol{M}_d = \frac{1}{\alpha}\begin{bmatrix} 1 & 0 \\ 0 & 1 \end{bmatrix} \Longrightarrow \boldsymbol{M}_d^{-1} = \alpha \begin{bmatrix} 1 & 0 \\ 0 & 1 \end{bmatrix}, \tag{21}$$

with $\alpha \in \mathbb{R}^+$ being a positive parameter. Subsequently, we are admitted to solve $\boldsymbol{\Lambda}_d$ from (19) and $P_d(\boldsymbol{e})$ from (20), respectively. Based on the structure of centripetal-Coriolis matrix $\boldsymbol{V}_m$ in (2), it follows that

$$\boldsymbol{\varphi}^{\perp}\boldsymbol{V}_m\dot{\boldsymbol{e}} = \begin{bmatrix} 0 & 1 \end{bmatrix}\begin{bmatrix} 0 & -ml\sin\theta\dot{\theta} \\ 0 & 0 \end{bmatrix}\begin{bmatrix} \dot{x} \\ \dot{\theta} \end{bmatrix} \equiv 0,$$

and hence (19) can be reduced to

$$-\boldsymbol{\varphi}^{\perp}\boldsymbol{M}(\boldsymbol{q})\boldsymbol{M}_d^{-1}\boldsymbol{\Lambda}_d\dot{\boldsymbol{e}} = 0.$$

Then, one feasible solution for $\boldsymbol{\Lambda}_d$ can be derived as

$$\boldsymbol{\Lambda}_d = \kappa \boldsymbol{M}_d\boldsymbol{M}^{-1}(\boldsymbol{q})\boldsymbol{\varphi}\boldsymbol{\Xi}, \tag{22}$$

wherein $\kappa \in \mathbb{R}^+$ is a positive damping gain. To guarantee that $\boldsymbol{\Lambda}_d$ is positive semi-definite, we take

$$\boldsymbol{\Xi} = \boldsymbol{\varphi}^{\mathrm{T}}T(\boldsymbol{M}_d\boldsymbol{M}^{-1})^{\mathrm{T}} = \boldsymbol{\varphi}^{\mathrm{T}}\boldsymbol{M}_d\boldsymbol{M}^{-1}.$$

By further substituting $\boldsymbol{M}(\boldsymbol{q})$ of (2) and $\boldsymbol{M}_d$ of (21) into (22), it is derived that

$$\begin{aligned}\boldsymbol{\Lambda}_d &= \frac{\kappa}{\alpha^2}\cdot\frac{1}{\det(\boldsymbol{M})}\begin{bmatrix} ml^2 & -ml\cos\theta \\ -ml\cos\theta & M+m \end{bmatrix}\cdot \\ &\quad \begin{bmatrix} 1 & 0 \\ 0 & 0 \end{bmatrix}\cdot\frac{1}{\det(\boldsymbol{M})}\cdot\begin{bmatrix} ml^2 & -ml\cos\theta \\ -ml\cos\theta & M+m \end{bmatrix} \\ &= \frac{\kappa m^2 l^2}{\alpha^2(\det(\boldsymbol{M}))^2}\underbrace{\begin{bmatrix} l^2 & -l\cos\theta \\ -l\cos\theta & \cos^2\theta \end{bmatrix}}_{\boldsymbol{H}},\end{aligned} \tag{23}$$

where

$$\det(\boldsymbol{M}) = ml^2(M + m\sin^2\theta) > 0$$

denotes the determinant of $\boldsymbol{M}(\boldsymbol{q})$. It is easy to check that

$$l^2 > 0,\ \ \det(\boldsymbol{H}) = l^2\cos^2\theta - l^2\cos^2\theta = 0,$$

which illustrates that $\boldsymbol{H}$ and further $\boldsymbol{\Lambda}_d$ are positive semi-definite. Consequently, the third term in the bracket of (17) is calculated as

$$\begin{aligned}\boldsymbol{M}(\boldsymbol{q})\boldsymbol{M}_d^{-1}\boldsymbol{\Lambda}_d\dot{\boldsymbol{e}} &= \kappa\boldsymbol{\varphi}\boldsymbol{\varphi}^{\mathrm{T}}\boldsymbol{M}_d\boldsymbol{M}^{-1}\dot{\boldsymbol{e}} \\ &= \frac{\kappa}{\alpha\det(\boldsymbol{M})}\begin{bmatrix} ml^2\dot{x} - ml\cos\theta\dot{\theta} \\ 0 \end{bmatrix}.\end{aligned} \tag{24}$$

Subsequently, we proceed to solve $P_d(\boldsymbol{e})$. Substituting the equations of (2), (3), and (21) into (20) yields the following expressions:

$$\begin{aligned}&\begin{bmatrix} 0 & 1 \end{bmatrix}\left\{\begin{bmatrix} 0 \\ mgl\sin\theta \end{bmatrix} - \begin{bmatrix} M+m & ml\cos\theta \\ ml\cos\theta & ml^2 \end{bmatrix}\right. \\ &\qquad \left.\cdot\begin{bmatrix} \alpha & 0 \\ 0 & \alpha \end{bmatrix}\begin{bmatrix} \frac{\partial P_d}{\partial e_x} \\ \frac{\partial P_d}{\partial\theta} \end{bmatrix}\right\} = 0 \Longrightarrow \\ &\begin{bmatrix} 0 & 1 \end{bmatrix}\begin{bmatrix} -\alpha(M+m)\frac{\partial P_d}{\partial e_x} - \alpha ml\cos\theta\frac{\partial P_d}{\partial\theta} \\ mgl\sin\theta - \alpha ml\cos\theta\frac{\partial P_d}{\partial e_x} - \alpha ml^2\frac{\partial P_d}{\partial\theta} \end{bmatrix} = 0,\end{aligned}$$

which results in the following partial differential equation:

$$\alpha\cos\theta\cdot\frac{\partial P_d(\boldsymbol{e})}{\partial e_x} + \alpha l\cdot\frac{\partial P_d(\boldsymbol{e})}{\partial\theta} - g\sin\theta = 0. \tag{25}$$

After solving (25), we can derive the following result:

$$P_d(\boldsymbol{e}) = -\frac{g}{\alpha l}\cos\theta + \Omega\left(-e_x + \frac{1}{l}\sin\theta\right), \tag{26}$$

where $\Omega(\cdot) \in \mathbb{R}$ represents an arbitrary scalar function. To guarantee that $P_d(\boldsymbol{e})$ is positive definite with respect to $e_x(t)$ and $\theta(t)$, $\Omega(\cdot)$ in (26) is chosen as

$$\Omega(\cdot) = \frac{g}{\alpha l} + k_p\ln\left[\cosh\left(e_x - \frac{1}{l}\sin\theta\right)\right], \tag{27}$$

with $k_p \in \mathbb{R}^+$ being a positive control gain yet to be introduced. Hence, $P_d(\boldsymbol{e})$ can be obtained from (26) and (27) as

$$P_d(\boldsymbol{e}) = \frac{g}{\alpha l}(1-\cos\theta) + k_p\ln\left[\cosh\left(e_x - \frac{1}{l}\sin\theta\right)\right], \tag{28}$$

which indicates that

$$\frac{\partial P_d(\boldsymbol{e})}{\partial e_x} = k_p \tanh\left(e_x - \frac{1}{l}\sin\theta\right), \tag{29}$$

$$\frac{\partial P_d(\boldsymbol{e})}{\partial \theta} = \frac{g}{\alpha l}\sin\theta - \frac{k_p}{l}\tanh\left(e_x - \frac{1}{l}\sin\theta\right)\cos\theta. \tag{30}$$

Thus, the fourth term in the bracket of (17) can be derived as

$$\boldsymbol{M}(\boldsymbol{q})\boldsymbol{M}_d^{-1}\frac{\partial P_d}{\partial \boldsymbol{e}} = \alpha\begin{bmatrix}(M+m)\frac{\partial P_d(\boldsymbol{e})}{\partial e_x} + ml\cos\theta\frac{\partial P_d(\boldsymbol{e})}{\partial\theta} \\ ml\cos\theta\frac{\partial P_d(\boldsymbol{e})}{\partial e_x} + ml^2\frac{\partial P_d(\boldsymbol{e})}{\partial\theta}\end{bmatrix}. \tag{31}$$

After substituting (2), (3), (8), (18), (24), (30), (29), and (31) into (17) and making some mathematical arrangements, the control law is finally obtained as[2]

$$\begin{aligned}F(t) =& -\alpha k_p(M + m\sin^2\theta)\tanh\left(e_x - \frac{1}{l}\sin\theta\right) \\ &- \frac{\kappa ml}{\alpha\det(\boldsymbol{M}(\boldsymbol{q}))}(l\dot{x} - \cos\theta\dot{\theta}) - mg\sin\theta\cos\theta \\ &- ml\sin\theta\dot{\theta}^2.\end{aligned} \tag{32}$$

The control law (32) can drive the system state to the equilibrium point, as will be supported by the theorem stated in the next section.

Remark 2 The introduction of the hyperbolic function $\tanh(\cdot)$ in $F(t)$ is of great benefit in the sense that it effectively reduces the initial control efforts, and thus guarantees smooth start of the cart. For zero initial conditions, i.e., $x(0) = 0,\ \dot{x}(0) = 0,\ \theta(0) = 0,\ \dot{\theta}(0) = 0 \Longrightarrow e_x(0) = -x_d$, the initial control efforts can be calculated from (32) as

$$\begin{aligned}|F(t)| &= |\alpha k_p M \cdot \tanh(-x_d)| \\ &\le \alpha k_p M \cdot \min\{|\cdot x_d|, 1\},\end{aligned}$$

wherein the last term is the initial control force for the case without saturation. Thus, if the desired cart position x_d is very far, that is, $|e_x(0)| = |-x_d| = x_d \gg 1$, the proposed controller can effectively reduce the initial control force and achieve soft start of the cart, which can hence effectively reduce the cart acceleration and avoid exciting large-amplitude load swing. In addition, the presented controller also reduces the control efforts during the overall transportation process, which will be demonstrated by both the simulation and the experimental results provided in Sect. 5.

Remark 3 It is worthwhile to point out that, for the partially saturated controller part, one can conveniently replace the hyperbolic tangent function $\tanh(\cdot)$ with other smooth saturated functions such as $\arctan(\cdot)$ and so on, with guaranteed stability and convergence properties.

Remark 4 Different from linear control systems, there are no general guidelines to select control gains with systematic procedures for nonlinear control systems such as cranes. After a lot of simulation and experimental tests, some rules are summarized at this point for choosing suitable parameters of the proposed controller. More precisely, the effects of k_p and κ are analogous to those of proportional and derivative gains in traditional proportional integral derivative (PID) control, respectively; therefore, one may borrow ideas from PID control tuning for selecting k_p and κ. The parameter α provides extra flexibility to tune the response of the control system, and we can set it as a specific positive constant value when choosing k_p and κ. Once k_p and κ are determined, we could further change the value of α to yield better system response.

4 Stability and performance analysis

We will illustrate the convergence of the closed-loop (objective system) signals together with the corresponding stability analysis using Lyapunov-based techniques. The following theorem holds for the proposed control law (32) that converts the crane dynamics into the objective system (10) with $\boldsymbol{M}_d$, $\boldsymbol{\Lambda}_d$, and $P_d(\boldsymbol{e})$ selected in (21), (23), and (28), respectively.

Theorem 1 *The objective system (10) is asymptotically stable at the equilibrium point, that is,*

$$\lim_{t\to\infty}\left[x(t)\ \dot{x}(t)\ \theta(t)\ \dot{\theta}(t)\right]^T = \left[x_d\ 0\ 0\ 0\right]^T.$$

[2] Owing to the smooth property, the hyperbolic tangent function $\tanh(\cdot)$ in the controller (32) does not affect the uniqueness and existence of the solutions of the closed-loop (objective) system.

Proof To prove this theorem, we substitute $P_d(\boldsymbol{e})$ of (28) into (11) to derive the Lyapunov function candidate as

$$V(t) = \frac{1}{2}\dot{\boldsymbol{e}}^{\mathrm{T}}\boldsymbol{M}_d\dot{\boldsymbol{e}} + k_p \ln\left[\cosh\left(e_x - \frac{1}{l}\sin\theta\right)\right] + \frac{g}{\alpha l}(1-\cos\theta) \geq 0. \tag{33}$$

Taking the time derivative of (33) along the trajectories of (10) directly indicates the result of (12). Then, using the expression (23), (12) can be rewritten as

$$\begin{aligned}\dot{V}(t) &= -\frac{\kappa m^2 l^2}{\alpha^2(\det(\boldsymbol{M}))^2}\dot{\boldsymbol{e}}^{\mathrm{T}}\begin{bmatrix} l^2 & -l\cos\theta \\ -l\cos\theta & \cos^2\theta \end{bmatrix}\dot{\boldsymbol{e}} \\ &= -\frac{\kappa m^2 l^2}{\alpha^2(\det(\boldsymbol{M}))^2}\cdot(l\dot{e}_x - \cos\theta\dot{\theta})^2 \leq 0. \end{aligned} \tag{34}$$

Therefore, the equilibrium point of the closed-loop system (10) is Lyapunov stable, and the following conclusions can be drawn from (7), (32), and (34):

$$e_x(t),\ \dot{e}_x(t)\ (\text{i.e.,}\ \dot{x}(t)),\ \dot{\theta}(t) \in \mathcal{L}_\infty \Longrightarrow x(t),\ F(t) \in \mathcal{L}_\infty. \tag{35}$$

To accomplish the proof, let $\mathcal{S}$ be defined as

$$\mathcal{S} \triangleq \left\{(x,\ \dot{x},\ \theta,\ \dot{\theta}) \mid \dot{V} = 0\right\}$$

and denote $\mathcal{M}$ as the largest invariant set in $\mathcal{S}$. Then, it can be shown from (34) that in $\mathcal{M}$

$$l\dot{e}_x - \cos\theta\dot{\theta} = 0 \Longrightarrow e_x - \frac{1}{l}\sin\theta = C_1, \tag{36}$$

where C_1 is a yet-to-be-determined constant. Before solving C_1, we substitute (6) into (5) and rearrange the resulting formula to produce

$$(M + m\sin^2\theta)\ddot{x} - mg\sin\theta\cos\theta - ml\dot{\theta}^2\sin\theta = F. \tag{37}$$

By substituting (32) into (37) and employing the conclusion of (36), one derives the following result:

$$\ddot{x} = -\alpha k_p \tanh(C_1). \tag{38}$$

It is evident from (38) that $\dot{x}(t)$ increases/decreases at the rate of $-\alpha k_p \tanh(C_1)$. If C_1 is a nonzero constant, then it indicates that $\dot{x}(t) = -\alpha k_p \tanh(C_1)\cdot t \to \infty$ as $t \to \infty$, which contradicts the fact of (35), so we can conclude that

$$C_1 = 0 \Longrightarrow \ddot{x} = -\alpha k_p \tanh(0) = 0. \tag{39}$$

Then, it follows from (38) that $\dot{e}_x(t) = C_2$ with C_2 being a constant. Performing some similar analyses with C_1, it can be shown that

$$\dot{e}_x = C_2 = 0 \Longrightarrow e_x = C_3, \tag{40}$$

where C_3 is a constant. Applying (39) to (36) yields

$$le_x = \sin\theta,$$

which, together with (6), (39), and (40), indicates that

$$\ddot{\theta} = -ge_x = -gC_3.$$

Then, if the constant C_3 is nonzero, $\dot{\theta}(t) \to \infty$ as $t \to \infty$, which apparently contradicts the conclusion of (35); consequently, $C_3 \neq 0$ is invalid. Thus, from (36) and (40), we have that

$$e_x = C_3 = 0 \Longrightarrow \sin\theta = 0. \tag{41}$$

By employing the practical assumption that $-\pi < \theta(t) < \pi$, it is concluded that[3]

$$\theta = 0 \Longrightarrow \dot{\theta} = 0. \tag{42}$$

On the basis of (40), (41), and (42), we conclude that the largest invariant set $\mathcal{M}$ contains only the equilibria. Then, it follows, by invoking LaSalle's invariance theorem [39], that the closed-loop system state variables are asymptotically convergent to the equilibrium point. □

5 Numerical simulation and hardware experiments

We will present some numerical simulation studies and hardware experimental results to confirm the practical performance of the proposed control method.

[3] It is worthwhile to point out that it is generally assumed that $-\pi/2 < \theta(t) < \pi/2$ [16–19,22,28,29], which means that the load will not go above the cart in practice. Hence in this sense, we have relaxed this assumption from a mathematical viewpoint, and an almost global asymptotic control result is obtained.

5.1 Numerical simulation

Through simulation studies, we intend to compare the control performance of the proposed method with the existing energy-based nonlinear controller in [20,21] expressed as follows:

$$F_{\rm nc} = \frac{-k_p e - k_d \dot{x} + k_v[\zeta(\theta,\dot{\theta}) - m\sin\theta\cos\theta\dot{\theta}\dot{x}]}{k_E + k_v}, \tag{43}$$

where k_p, k_d, k_v, and $k_E \in \mathbb{R}^+$ are positive control gains and $m(\theta) = M + m\sin^2\theta$, $\zeta(\theta,\dot{\theta}) = -m\sin\theta(l\dot{\theta}^2 + g\cos\theta)$.

The crane system's physical parameters in the simulation are configured as follows:

$$M = 4\ \text{kg},\ m = 2.5\ \text{kg},\ l = 1.5\ \text{m},\ g = 9.8\ \text{m/s}^2.$$

The control gains for both controllers are carefully tuned until their respective best performance is achieved, where the gains for the proposed controller are given as $k_p = 1.1$, $\alpha = 1$, $\kappa = 40$ and those for the nonlinear controller (43) are $k_p = 25, k_d = 50.5, k_E = 1$, and $k_v = 1.5$.

To show the advantage of the proposed controller, we implement 3 groups of simulation studies in total. In the *1st group*, the desired cart positions are set as $x_d = 1$ m, $x_d = 2$ m, and $x_d = 4$ m, respectively. Then in the *2nd group*, we replace the desired location $x_d = 2$ m with a converging trajectory given as

$$x_d(t) = 2(1 - \mathrm{e}^{-8.33t^3})\ [\text{m}]. \tag{44}$$

Finally, in the *3rd group*, we test the robustness of the proposed method, where the desired cart position is $x_d = 2$ m. The corresponding simulation results are given in Figs. 1, 2, 3, and 4.

The 1st Group It is clearly seen from Figs. 1 and 2 that for all three cases (the shorter distance $x_d = 1$ m, $x_d = 2$ m, and the longer distance $x_d = 4$ m), the proposed controller achieves better control performance (smaller load swing) than the nonlinear controller (43) with much less control efforts. Though the transportation time for the energy-based method (43) is similar in the three studies, the paid price is that the (initial) control efforts (see the partially zoomed-in plot in Fig. 1) and the load swing angles increase sharply with longer transportation distance (the swing angle even reaches as much as almost 30°), which is dangerous and unexpected in practice. By contrast, the proposed control method achieves "soft" load transportation with well-suppressed load swing (less than 5°), as clearly shown in Fig. 2, which is beneficial in real-world applications.

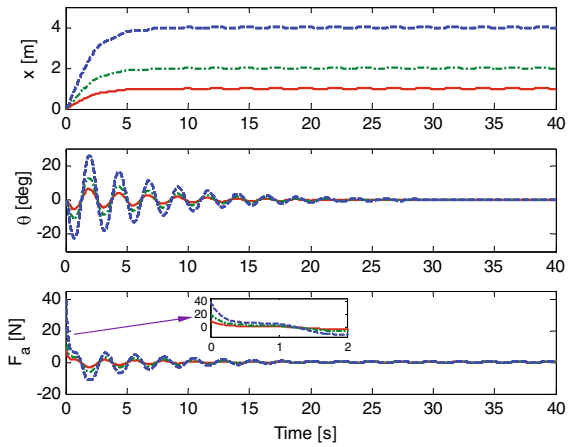

Fig. 1 The 1st group: simulation results for the nonlinear controller (43) (*solid line* $x_d = 1$ m; *dotted-dashed line* $x_d = 2$ m; *dashed line* $x_d = 4$ m)

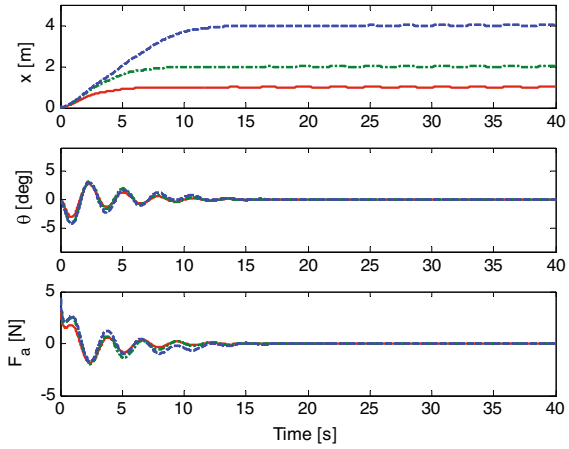

Fig. 2 The 1st group: simulation results for the proposed controller (32) (*solid line* $x_d = 1$ m; *dotted-dashed line* $x_d = 2$ m; *dashed line* $x_d = 4$ m)

It should be noted that, for load transportation of different distances, one may reduce the load swing of the energy-based controller (43) by retuning the control gains at the expense of longer transportation time. Nonetheless, it is a cumbersome work since there are currently no general gain tuning guidelines for nonlinear control systems. Hence, it is another advantage of the proposed control system by noting that the same set of control gains work well for different distance transportation processes, as is clearly illustrated in Fig. 2.

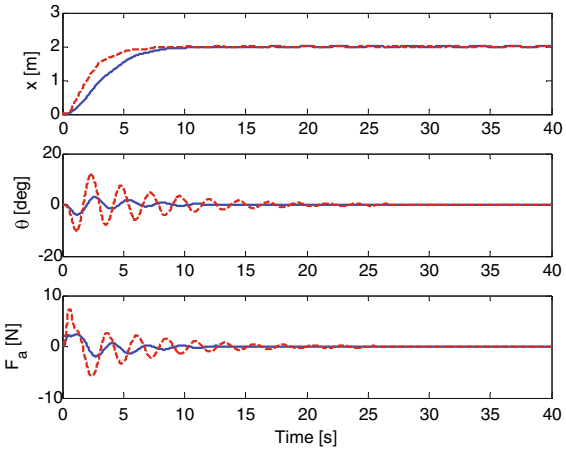

Fig. 3 The 2nd group: simulation results (*solid line* the proposed controller (32); *dashed line* the nonlinear controller (43))

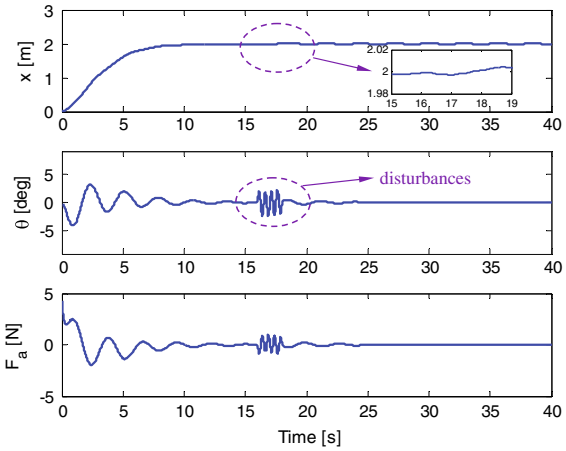

Fig. 4 The 3rd group: simulation results subject to disturbances

The 2nd Group In this group, we preliminarily validate the performance of the proposed method in the case of trajectory tracking, where the trajectory (44) is used. From Fig. 3, one can clearly see that the proposed controller (32) (solid line) still performs much more satisfactorily, in the tracking case, than the energy-based one (dotted line) [20,21], with similar transferring efficiency and much less control efforts.

The 3rd Group The robustness of the proposed approach with respect to disturbances is verified. To do so, we add sinusoid disturbances (amplitude: 2°, period: 0.5 s) to the load swing between 16 and 18 s. The response of the control system is depicted in Fig. 4, from which we can find that the disturbances are got rid of rapidly. This shows that the proposed method works well in the presence of external disturbances.

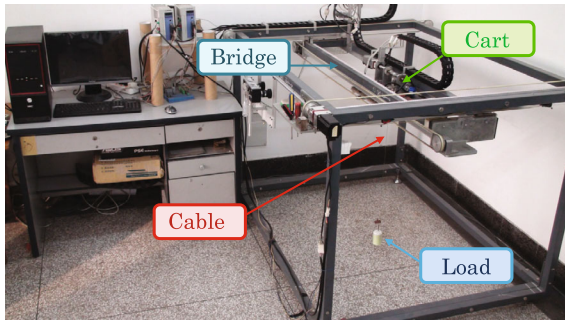

Fig. 5 The hardware gantry crane testbed

5.2 Hardware experimental verification

We will further present some experimental results to validate the performance of the proposed control approach. The experiments are implemented on a gantry crane testbed as shown in Fig. 5 (see also [15,22,35] for some descriptions regarding the testbed), where the physical parameters are configured as

$$M = 6.5 \text{ kg},\ m = 1 \text{ kg},\ l = 0.75 \text{ m},\ g = 9.8 \text{ m/s}^2. \tag{45}$$

We set the desired cart location as $x_d = 0.6$ m. The friction parameters in (4) are determined, after offline experimental calibration, as [15,22]

$$F_{r0} = 4.4,\ \varepsilon = 0.01,\ k_r = -0.5.$$

The control gains are carefully chosen for the proposed controller (32) as $k_p = 2.8$, $\alpha = 1$, $\kappa = 44$, and for the nonlinear controller (43) as $k_p = 60$, $k_d = 7.5$, $k_E = 1.2$, and $k_v = 1.8$. For control implementation, the MATLAB/SIMULINK RTWT running under Windows XP is utilized with the control period as 5 ms. We implement 2 sets of experiments to verify the performance of the proposed controller in the case of exact system model knowledge and uncertain system model knowledge, respectively.

The 1st Set—Exact System Model Knowledge The system parameters M, m, and l in controllers (32) and (43) are set the same with those in (45). The corresponding experimental results are presented from Figs. 6 to 7. To make the experimental results more understood, we also provide some quantified results, as shown in

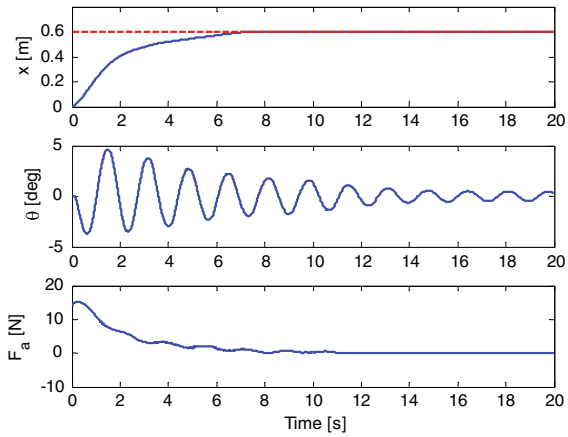

Fig. 6 The 1st set (exact system model knowledge): experimental results for the nonlinear controller (43) (*dashed line* $x_d = 0.6$ m)

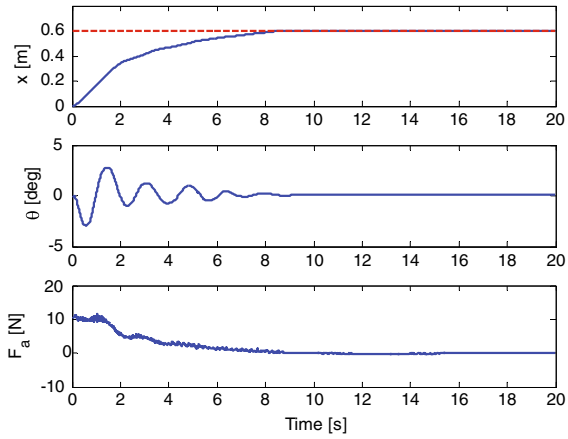

Fig. 7 The 1st set (exact system model knowledge): experimental results for the proposed controller (32) (*dashed line* $x_d = 0.6$ m)

Table 1; x_f denotes the final cart location, $\theta_{\max}$ denotes the maximum swing amplitude, θ_{r} denotes residual swing (referring to the maximum swing amplitude after 8 s), $\max\{|F_{\mathrm{a}}(t)|\}$ represents the maximum actuating force amplitude, and $\int_0^{20} F_{\mathrm{a}}^2(t)\mathrm{d}t$ is used to depict the consumed energy [36].

With regard to the transferring efficiency, it is observed from Figs. 6 and 7 and Table 1 that both control schemes drive the cart to reach the desired location accurately within about 8 s. Yet, the proposed controller suppresses the load swing to a smaller range and eliminates the residual swing more efficiently than the nonlinear controller (43). The improved control performance is brought about by the enhanced internal coupling between the cart motion and load swing, which benefits from the elaborately designed structure of the objective system (10). Further exploring the experimental results, one can see that the control efforts of the proposed control law, especially at the beginning, are much smaller due to the benefit of the introduction of the $\tanh(\cdot)$ function, whose saturated feature effectively reduces the initial control force and correspondingly decreases the energy consumption.

Remark 5 It is noted that the control efforts in the experiments are a bit different from those in the simulation studies, in terms of amplitudes and shapes. This is due to that the nonlinear friction force, which greatly influences the actuating input, was not considered in the simulation studies. On the other hand, it is observed that the load swing amplitude (corresponding to $x_d = 2$ m) in the simulation studies is similar to that (corresponding to $x_d = 0.6$ m) in the experiments. This also makes sense because the cable in the simulations ($l = 1.5$ m) is set much longer than that ($l = 0.75$ m) in the experiments, and longer cable length can reduce the load swing amplitude from a potential energy viewpoint [$\theta(t)$ decreases as l increases for the same potential energy $mgl(1 - \cos\theta)$].

The 2nd set—uncertain system model knowledge As a means to test the robustness of the designed control system, the system physical parameters (load mass m and cable length l) are changed as $m = 1.5$ kg, and $l = 0.8$ m, while in (32) we still use the parameters (i.e., the nominal values $m = 1$ kg, and $l = 0.75$ m); and the control gains in the 1st set of experiments. The

Table 1 Quantified experimental results (corresponding to Figs. 6, 7, and 8)

Controllers	x_f (m)	$\theta_{\max}$ (°)	θ_t (°)	$\max\{\|F_{\mathrm{a}}(t)\|\}$ (N)	$\int_0^{20} F_{\mathrm{a}}^2(t)\mathrm{d}t$ (N^2 · s)
Controller (43) in the 1st set	0.598	4.57	1.77	15.33	313.30
Proposed controller (32) in the 1st set	0.597	2.91	0.22	11.51	228.73
Proposed controller (32) in the 2nd set	0.598	2.96	0.51	11.83	293.36

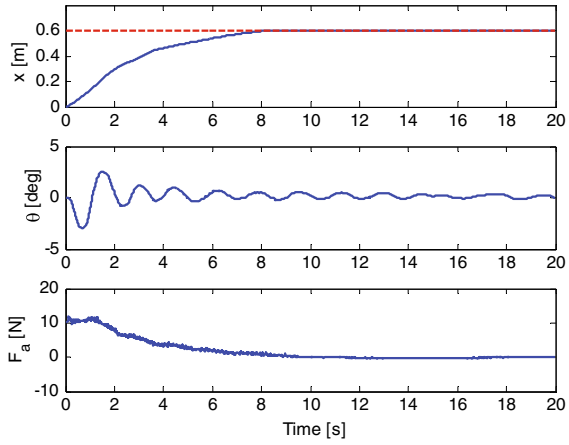

Fig. 8 The 2nd set (uncertain system model knowledge): experimental results for the proposed controller (32) (*dashed line* $x_d = 0.6$ m)

experimental results are shown in Fig. 8 and Table 1. It can be seen that even in the presence of parameter uncertainties, the proposed controller still achieves satisfactory cart positioning and swing suppression performance. This experiment indicates that the proposed control system shows good robustness to parameter uncertainties.

6 Conclusion and discussion

This paper has presented a partially saturated nonlinear control strategy for underactuated gantry cranes, by converting the crane dynamics into an objective system with guaranteed control performance. Due to the specific structure of the constructed objective system, the controller is obtained quite straightforwardly by solving one partial differential equation. Moreover, a smooth hyperbolic tangent function is introduced in the control structure to ensure "soft" cart start and reduce the control efforts. Both numerical and experimental results are presented to illustrate the increased control performance of the proposed scheme with respect to that of the existing energy-based controllers. In the future, we will attempt to extend the method to gantry cranes of higher dimensions in the presence of load hoisting/lowering.

Acknowledgments The authors would like to express their sincere thanks to the reviewers and the editor for the valuable suggestions that have greatly improved the quality of the paper. They also greatly acknowledge the financial supports from the National Science and Technology Pillar Program of China (Grant No. 2013BAF07B03), the National Science Fund for Distinguished Young Scholars of China (Grant No. 61325017), the National Natural Science Foundation of China (Grant No. 11372144), and the Academic Award for Doctoral Students from the Ministry of Education of China (Grant No. (190)H0511009).

References

1. Abdel-Rahman, E.M., Nayfeh, A.H., Masoud, Z.N.: Dynamics and control of cranes: a review. J. Vib. Control **9**(7), 863–908 (2003)
2. Li, Y., Liu, Y.: Real-time tip-over prevention and path following control for redundant nonholonomic mobile modular manipulators via fuzzy and neural-fuzzy approaches. ASME J. Dyn. Syst. Meas. Control **128**(4), 753–764 (2006)
3. Liu, Y., Li, Y.: Dynamic modeling and adaptive neural-fuzzy control for nonholonomic mobile manipulators moving on a slope. Int. J. Control Autom. Syst. **4**(2), 197–203 (2006)
4. Ouyang, H., Uchiyama, N., Sano, S.: Anti-sway control of rotary crane only by horizontal boom motion. In: Proceedings of the 2010 IEEE International Conference on Control Applications, Yokohama, Japan, pp. 591–595 (2010)
5. Xin, X., She, J., Liu, Y.: A unified solution to swing-up control for n-link planar robot with single passive joint based on virtual composite links and passivity. Nonlinear Dyn. **67**(2), 909–923 (2012)
6. Kuchler, S., Mahl, T., Neupert, J., Schneider, K., Sawodny, O.: Active control for an offshore crane using prediction of the vessel's motion. IEEE/ASME Trans. Mechatron. **16**(2), 297–309 (2011)
7. She, J.H., Zhang, A., Lai, X., Wu, M.: Global stabilization of 2-DOF underactuated mechanical systems: an equivalent-input-disturbance approach. Nonlinear Dyn. **69**(1–2), 495–509 (2012)
8. Li, E., Liang, Z.Z., Hou, Z.G., Tan, M.: Energy-based balance control approach to the ball and beam system. Int. J. Control **82**(6), 981–992 (2009)
9. Ibañez, C. A., García, J. C. M., López, A. S.: Bounded control based on saturation functions of nonlinear underactuated mechanical systems: the cart-pendulum system case. In: Proceedings of the 50th IEEE Conference on Decision and Control and European Control Conference, Orlando, USA, pp. 1759–1764 (2011)
10. Gao, B.T., Xu, J., Zhao, J.G., Huang, X.L.: Stabilizing control of an underactuated 2-dimensional TORA with only rotor angle measurement. Asian J. Control **15**(3), 1–12 (2013)
11. Xin, X., She, J.H., Yamasaki, T., Liu, Y.: Swing-up control based on virtual composite links for n-link underactuated robot with passive first joint. Automatica **45**(9), 1986–1994 (2009)
12. Piazzi, A., Visioli, A.: Optimal dynamic-inversion-based control of an overhead crane. IEE Proc. Control Theory Appl. Part D **149**(5), 405–411 (2002)
13. Van den Broeck, L., Diehl, M., Swevers, J.: A model predictive control approach for time optimal point-to-point motion control. Mechatronics **21**(7), 1203–1212 (2011)

14. Sun, N., Fang, Y., Zhang, X., Yuan, Y.: Phase plane analysis based motion planning for underactuated overhead cranes. In: Proceedings of the 2011 IEEE International Conference on Robotics and Automation, Shanghai, China, pp. 3483–3488 (2011)
15. Sun, N., Fang, Y., Zhang, X., Yuan, Y.: Transportation task-oriented trajectory planning for underactuated overhead cranes using geometric analysis. IET Control Theory Appl. **6**(10), 1410–1423 (2012)
16. Khalid, A., Huey, J., Singhose, W., Lawrence, J., Frakes, D.: Human operator performance testing using an input-shaped bridge crane. ASME J. Dyn. Syst. Meas. Control **128**(4), 835–841 (2006)
17. Garrido, S., Abderrahim, M., Giménez, A., Diez, R., Balaguer, C.: Anti-swinging input shaping control of an automatic construction crane. IEEE Trans. Autom. Sci. Eng. **5**(3), 549–557 (2008)
18. Masoud, Z.N., Nayfeh, A.H.: Sway reduction on container cranes using delayed feedback controller. Nonlinear Dyn. **34**(3–4), 347–358 (2003)
19. Solihin, M.I., Wahyudi, Legowo, A.: Fuzzy-tuned PID anti-swing control of automatic gantry crane. J. Vib. Control **16**(1), 127–145 (2010)
20. Fang, Y., Zergeroglu, E., Dawson, D.M., Dixon, W.E.: Nonlinear coupling control laws for an overhead crane system. In: Proceedings of the IEEE Conference on Control Applications, Mexico City, Mexico, pp. 639–644 (2001)
21. Fang, Y., Dixon, W.E., Dawson, D.M., Zergeroglu, E.: Nonlinear coupling control laws for an underactuated overhead crane system. IEEE/ASME Trans. Mechatron. **8**(3), 418–423 (2003)
22. Sun, N., Fang, Y., Zhang, Y., Ma, B.: A novel kinematic coupling-based trajectory planning method for overhead cranes. IEEE/ASME Trans. Mechatron. **17**(1), 166–173 (2012)
23. Sun, N., Fang, Y.: An efficient online trajectory generating method for underactuated crane systems. Int. J. Robust Nonlinear Control. doi:10.1002/rnc.2953 (in press)
24. Liu, R., Li, S., Ding, S.: Nested saturation control for overhead crane systems. Trans. Inst. Meas. Control **34**(7), 862–875 (2012)
25. Burg, T., Dawson, D., Rahn, C., Rhodes, W.: Nonlinear control of an overhead crane via the saturating control approach of Teel. In: Proceedings of the 1996 IEEE International Conference on Robotics and Automation, Minneapolis, USA, pp. 3155–3160 (1996)
26. Wang, W., Yi, J., Zhao, D., Liu, D.: Design of a stable sliding-mode controller for a class of second-order underactuated systems. IEE Proc. Control Theory Appl. Part D **151**(6), 683–690 (2004)
27. Bartolini, G., Pisano, A., Usai, E.: Second-order sliding-mode control of container cranes. Automatica **38**(10), 1783–1790 (2002)
28. Ngo, Q.H., Hong, K.-S.: Adaptive sliding mode control of container cranes. IET Control Theory Appl. **6**(5), 662–668 (2012)
29. Lee, H., Liang, Y., Segura, D.: A sliding-mode antiswing trajectorycontrol for overhead cranes with high-speed load hoisting. ASME J. Dyn. Syst. Meas. Control **128**(4), 842–845 (2006)
30. Park, M.S., Chwa, D., Hong, S.K.: Antisway tracking control of overhead cranes with system uncertainty and actuator nonlinearity using an adaptive fuzzy sliding-mode control. IEEE Trans. Ind. Electron. **55**(11), 3972–3984 (2008)
31. Le, T.A., Kim, G.-H., Kim, K.Y., Lee, S.-G.: Partial feedback linearization control of overhead cranes with varying cable lengths. Int. J. Precis. Eng. Manuf. **13**(4), 501–507 (2012)
32. Liu, D., Guo, W., Yi, J.: Dynamics and GA-based stable control for a class of underactuated mechanical systems. Int. J. Control Autom. Syst. **6**(1), 35–43 (2008)
33. Toxqui, R., Yu, W., Li, X.: Anti-swing control for overhead cranes with neural compensation. In: Proceedings of the International Joint Conference on Neural Networks, Vancouver, Canada, pp. 9447–9453 (2006)
34. Chang, C.: Adaptive fuzzy controller of the overhead cranes with nonlinear disturbance. IEEE Trans. Ind. Inf. **3**(2), 164–172 (2007)
35. Ma, B., Fang, Y., Zhang, Y.: Switching-based emergency braking control for an overhead crane system. IET Control Theory Appl. **4**(9), 1739–1747 (2010)
36. Hu, G., Makkar, C., Dixon, W.E.: Energy-based nonlinear control of underactuated Euler–Lagrange systems subject to impacts. IEEE Trans. Autom. Control **52**(9), 1742–1748 (2007)
37. Ortega, R., Spong, M.W., Gómez-Estern, F., Blankenstein, G.: Stabilization of a class of underactuated mechanical systems via interconnection and damping assignment. IEEE Trans. Autom. Control **47**(8), 1218–1233 (2002)
38. Makkar, C., Hu, G., Sawyer, W.G., Dixon, W.E.: Lyapunov-based tracking control in the presence of uncertain nonlinear parameterizable friction. IEEE Trans. Autom. Control **52**(10), 1988–1994 (2007)
39. Khalil, H.K.: Nonlinear Systems, 3rd edn. Prentice-Hall, Englewood Cliffs (2002)